- 1 This version of the article has been accepted for publication, after peer review and is subject to Springer
- 2 Nature's AM terms of use, but is not the Version of Record and does not reflect post-acceptance
- 3 improvements, or any corrections. The Version of Record is available online
- 4 at: <a href="http://dx.doi.org/10.1038/s41586-024-07518-6">http://dx.doi.org/10.1038/s41586-024-07518-6</a>

10

11

12

13

14

15

16

17

18

19

20

21

22

23

24

- 5 Fault Network Geometry Influences Earthquake Frictional Behavior
- 6 Jaeseok Lee<sup>1</sup>, Victor C. Tsai<sup>1\*</sup>, Greg Hirth<sup>1</sup>, Avigyan Chatterjee<sup>2</sup>, Daniel T. Trugman<sup>2</sup>
- 7 1 Department of Earth, Environmental, and Planetary Sciences, Brown University
- 8 2 Nevada Seismological Laboratory, University of Nevada, Reno

Understanding the factors governing the stability of fault slip is a crucial problem in fault mechanics<sup>1-3</sup>. The importance of fault geometry and roughness on fault-slip behaviour has been highlighted in recent lab experiments<sup>4-7</sup> and numerical models<sup>8-11</sup>, and emerging evidence suggests that large-scale complexities in fault networks play a vital role in the faultrupture process<sup>12–18</sup>. Here we present a new perspective on fault creep by investigating the link between fault-network geometry and surface creep rates in California, USA. Our analysis reveals that fault groups exhibiting creeping behaviour show smaller misalignment in their fault-network geometry. The observation indicates that the surface fault traces of creeping regions tend to be simple, whereas locked regions tend to be more complex. We propose that the presence of complex fault-network geometries results in geometric locking that promotes stick-slip behaviour characterized by earthquakes, whereas simpler geometries facilitate smooth fault creep. Our findings challenge traditional hypotheses on the physical origins of fault creep explained primarily in terms of fault friction 19-21 and demonstrate the potential for a new framework in which large-scale earthquake frictional behaviour is determined by a combination of geometric factors and rheological yielding properties.

The mechanisms that govern fault creep remain a topic of debate. The stability of fault slip is typically attributed to frictional parameters of the rate-and-state law<sup>19-21</sup>, and fault creep has been linked to factors including low shear strength of fault materials<sup>22-24</sup> and increased pore pressure<sup>25,26</sup> within this framework. However, recent studies also emphasize the potential importance of fault geometry on fault slip behavior. Laboratory experiments and numerical models have highlighted the importance of fault plane roughness, although there are divergent interpretations on whether rough faults promote or suppress stable sliding<sup>4-7,10</sup>. Studies based on InSAR and GPS observations have demonstrated fault creep in segments with simple fault geometries<sup>27,28</sup>, creep promoted by heterogeneous stress fields resulting from fault roughness<sup>29</sup>, and variable creep rates associated with local fault strike and regional stress orientations<sup>30-32</sup>. Given the diverse evidence and lack of consensus, a comprehensive understanding of fault creep remains elusive<sup>2</sup>.

Recent findings suggest that the often-overlooked effects of larger-scale complexities in fault networks, such as bends, gaps and stepovers, play a pivotal role in the earthquake rupture process<sup>9,12-18</sup>. Geometric complexities in fault systems give rise to localized stress concentrations, which can either facilitate or impede earthquake rupture initiation and arrest. However, given the difficulties of including large-scale fault complexities in standard numerical earthquake rupture models, there has been limited research on the impact of such geometric complexity. We propose that the geometrical complexity of fault networks can have a significant role in suppressing fault creep, and establish a quantitative connection between the two through observations. We test the correlation between quantitative metrics of fault network geometry<sup>15</sup> and measurements of surface creep rate along some of the major fault zones in California. We find that statistical metrics of geometrical fault network complexity have strong explanatory power for the occurrence of fault creep.

# **Fault Complexity and Creep Measurements**

California has extensively documented fault creep. Large surface creep rates of about 30 mm/year are observed along the central section of the San Andreas Fault, and surface creep rates of about 5 mm/year are observed along the creeping sections of the Maacama, Calaveras, Bartlett-Springs, Coachella, Hayward, and Superstition Hills fault segments<sup>33</sup>. While there is no unified perspective to explain the spatial variation in why some faults exhibit creep while others remain locked, understanding the key factors driving fault creep is essential for analyzing fault slip behavior and its implications for seismic events in California and beyond. Here we test the hypothesis that the spatial variability in creep can be explained in terms of large-scale fault complexity, using high-resolution fault maps from the USGS Ouaternary Fault Database<sup>34</sup>.

As detailed in the Methods section, we quantify fault network complexity by measuring the degree of fault misalignment and fault density along these documented fault segments and explore their connections with surface creep rates. For a fractal fault geometry, fault misalignment remains independent of fault map resolution, making it a robust indicator of fault complexity, whereas fault density is resolution dependent<sup>15</sup> (see Methods). The spatial pattern of fault misalignment is diverse, ranging from 0.1 to 0.8 across California (Fig. 1). The largest fault misalignments of 0.6 to 0.8 are observed in complex fault zones, such as the region near the southern tip of the San Jacinto Fault, or in areas where major fault zones intersect, as in the Big Bend area. The smallest fault misalignments, ranging between 0.1 and 0.2, are in regions where fault strands predominantly run parallel to each other. Examples of such regions include a ~120-km segment along the Central San Andreas Fault, as well as areas along the Maacama and Hayward faults. Importantly, these measurements involve intersecting fault strands between

networks of faults at scales ranging from 10 to 15 kilometers. These measurements are distinct from the highly localized, sub-kilometer scale fault geometry features related to fault damage zones<sup>35</sup> or fault roughness<sup>36,37</sup>.

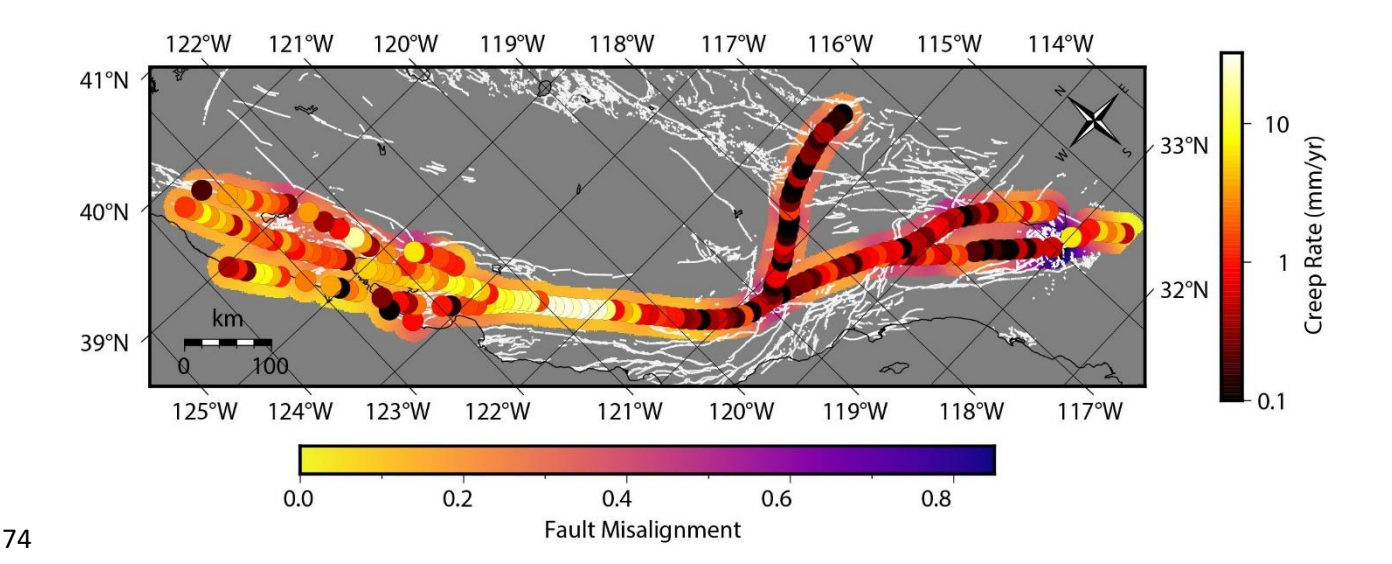


**Figure 1.** Fault misalignment and surface creep rates along major faults in California. Surface fault traces from the USGS Quaternary Faults Database plotted in white, with fault misalignments as colored background and creep rates as colored circles. Fault misalignments calculated within 15-km radius circles are shown using 25-km radius circles here for clarity.

A low degree of fault misalignment is generally observed in many regions with significant surface creep rates. A negative correlation between creep rates and fault misalignment is observed with a rank correlation coefficient of -0.35 (Extended Data Fig. 1a). We further quantify this by categorizing the slip behavior into either "locked" or "creeping" based on the absolute values of the estimated creep rates. We find a distinct difference in these two categories, with fault misalignment being larger along locked sections of faults compared to creeping sections (Fig. 2a). The average value of misalignment is 0.28 for the locked sections and 0.19 for the creeping sections, with standard deviations of 0.13 and 0.11 respectively. This observation indicates that,

with respect to the orientation of surface fault traces, creeping regions tend to be simple, whereas locked regions tend to be more complex. A two-sample Kolmogorov–Smirnov test of the fault misalignment distribution between locked and creeping fault sections rejects the null hypothesis that the two distributions are identical with a confidence level of 99.9%. These findings extend the qualitative explanations made for fault creep at individual fault sections with simple fault geometries<sup>27,28</sup> to a broader analysis for the entire California region. Our study focuses on California due to the availability of detailed creep measurements and fault network maps, but other fault systems with sufficient data quality and resolution, such as the North Anatolian Fault and the Chaman Fault, also demonstrate negative correlations between fault network misalignment and surface creep rates (Extended Data Fig. 2). The consistent negative correlations observed in other creeping faults globally indicate that the influence of fault complexity on fault creep may be a universal behavior.

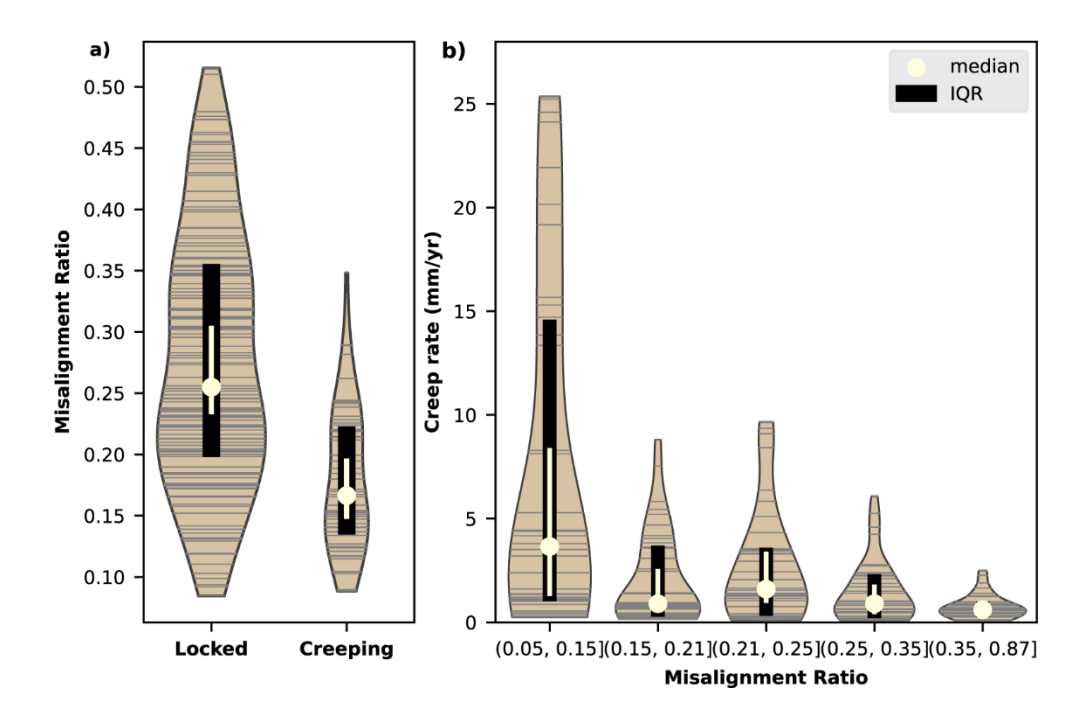


**Figure 2.** Fault misalignment versus creep rates. **a**, Violin plot of fault misalignments according to whether the surface creep rates indicate locked or creeping. **b**, Violin plot of surface creep rates

according to fault misalignments binned in five quantile bins. Black bars indicate 1st and 3rd quartile bounds, and the yellow circles indicate median values within each bin, with yellow error bars indicating 95% confidence intervals. In a, 60 data points are categorized as creeping and 148 data points are categorized as locked. Violin plots exclude 2.5% outliers at both ends, showing 95% of the distributions, and horizontal ticks indicate data points.

When examining the distribution of surface creep rates grouped into five quantiles bins of increasing fault misalignment, we find that large surface creep rates are observed almost exclusively in regions of small misalignment ratio (Fig. 2b). For example, in the lowest quantile bin of fault misalignment, 40% of the associated creep rates surpass 5 mm/year, while only 12% of the data exceed the same threshold in the remaining bins on average. This implies that fault creep is considerably more probable along fault sections where the misalignment ratio is below 0.15. However, not all simple faults exhibit creep - there are data points where a low surface creep rate (or locking) is measured at low misalignments, suggesting that other physics beyond geometry plays a competing role. While locked fault sections are present in all five quantile bins, the percentage of locked faults in each bin relative to the total number of locked faults increases with fault misalignment. In ascending order of misalignment, 12.2%, 18.2%, 18.2%, 24.3%, and 27.0% of creep rates lower than 3 mm/year are found in each bin. This observation indicates that locked faults are more prevalent in regions with more misaligned fault networks. Furthermore, the negative correlations remain consistent when applying the same analysis to normalized creep rates (see Extended Data Fig. 1b) or when grouping the data by fault systems (see Extended Data Fig. 3).

102

103

104

105

106

107

108

109

110

111

112

113

114

115

116

117

118

119

120

121

# **Implications for Fault Slip Behavior**

124

125

126

127

128

129

130

131

132

133

134

135

136

137

138

139

140

141

142

143

144

145

146

We have introduced and demonstrated a potential relationship between fault network complexity and surface creep rates, an idea that has not been explored previously. Fault network misalignment does not account for all of the observed variability in creep rates. However, robust correlations between fault creep behavior and properties such as heat flow, gouge mineralogy and pore-fluid pressure are hard to assess owing to the difficulty in resolving the local fault-scale properties at depth. Our findings indicate that the accommodation of regional stress loading in large-scale geometrical incompatibilities may be a primary controlling factor on the seismogenic nature of faults. Furthermore, our work suggests that unstable slip behavior is influenced by the response of the entire fault system, not solely by the properties of a planar slip surface. The mechanisms governing the rupture process in complex fault networks may be entirely different from simple frictional sliding or frictional resistance caused by on-fault asperities. Unlike microscale asperities or fault roughness, which can be overcome through elastic/plastic deformation, larger fault network complexities are features that are difficult to overcome through either mechanism<sup>38</sup>. Our analyses intimate that fault network complexities function as geometric incompatibilities that significantly suppress steady fault motion as 'geometric asperities'. The instability of complex geometries may arise because the rupturing of geometrically locked surfaces involves inherently unstable physical processes like the elastic unmating of surfaces<sup>17</sup> or fracture<sup>39</sup>. whereas surficial frictional processes are more stable<sup>40</sup>. Within such a framework, we suggest that locked faults are found more frequently in fault systems with complex geometry, while faults with simpler geometries are more prone to steady creep. It is difficult to determine the precise control of fault geometry on the fault slip behavior, but we anticipate an intermediate behavior between stable sliding and stick-slip behavior in real fault networks with intersecting fault strands of varying sizes, and this may be a reason for some of the uncertainty in the observed correlations at the scale of our reported observations. The frictional behavior of fault networks may demonstrate a wide range of behaviors primarily controlled by the fault network geometry, but also influenced by local properties of individual fault segments. Depending on the interaction of geometric complexities and frictional properties of fault segments, faults may: (a) rupture together as a large complex system<sup>41,42</sup>, (b) undergo significant regional deformation<sup>43</sup>, or (c) simply creep under the background stress loading<sup>44</sup>. It is also possible that creeping aligned fault regions become seismogenic and undergo rapid slip when nearby complex junctions yield.

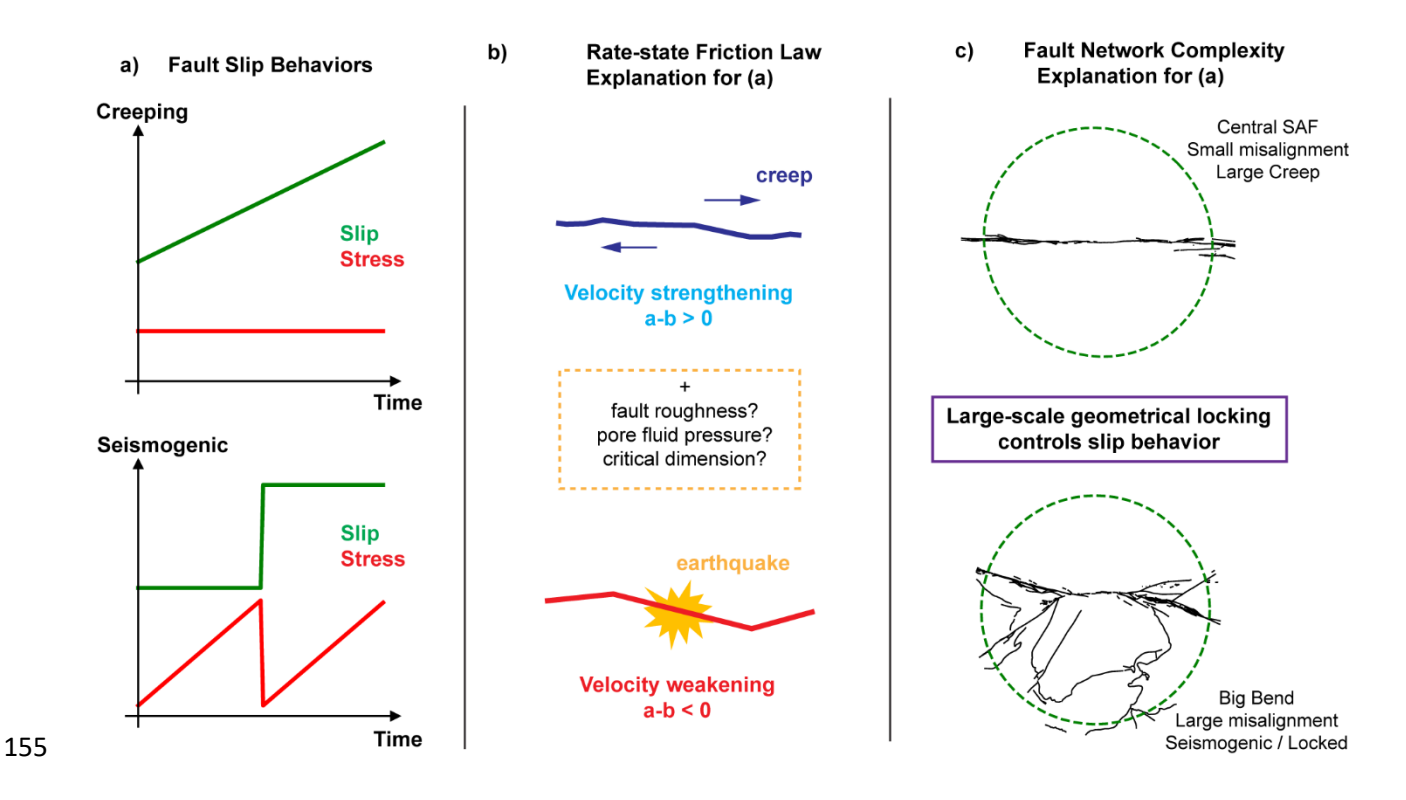


**Figure 3.** Schematic illustrations of explanations of seismogenic behavior. **a**, Two distinct fault slip behaviors, creeping and seismogenic. **b**, The standard rate-and-state friction framework explanation. **c**, Our explanation of how we propose fault geometry controls fault creep.

Our hypothesis suggesting that the large-scale frictional behavior of faults is influenced by the complex geometry of fault networks could illuminate the interaction between friction and fault system geometry that has been overlooked in traditional perspectives based on microscopic laboratory-derived rate-and-state frictional parameters. It has been the general understanding that either geometric or material complexities controlling slip behavior are limited to localized properties, and dynamic earthquake simulations have aimed to reproduce fault slip characteristics mostly within this framework<sup>45</sup>. Smooth and stable sliding of creeping faults has been modeled to result from velocity-strengthening friction behavior coupled with factors such as fault roughness, rheological properties, pore-fluid pressure, and critical slip distance. Earthquakes, on the other hand, have been thought to occur due to the instability of friction on faults with velocity-weakening behavior. Our study introduces a new perspective on earthquake behavior, highlighting the significance of slip resistance caused by geometric incompatibilities rather than variations in laboratory-measured frictional properties (Fig. 3). Our findings suggest that the characterization of stick-slip frictional behavior may be better achieved through measurements of fault geometry together with yielding material properties rather than relying solely on smooth-fault friction experiments, indicating potential future directions for earthquake rupture modeling.

159

160

161

162

163

164

165

166

167

168

169

170

171

172

173

174

175

176

177

178

179

180

181

While we have primarily concentrated on understanding how fault complexity controls fault stability, the two can influence each other in a complex way. For example, dilatation can be observed in the transition zones from creeping to locked, which can generate new local fractures and increase both the density and misalignment of faults<sup>46</sup>. In addition, when earthquakes are hosted in locked regions with significant complexity, breakthrough of faults may be required to overcome the geometric incompatibilities. Thus, some complex regions may become even more complex, at odds with the traditional view that fault systems only get simpler as they mature.

Moreover, the presence or removal of significant geometric features may promote a transition from seismogenic to creeping behavior, and vice versa. As an example, the removal of a geometric complexity initially triggering a mainshock could explain post-seismic fault creep, and initiation of changes in long-term creep behavior may require the re-organization of fault system geometry over geologic time. This implies that seismogenic and creeping behavior may coexist on a single fault segment due to geometric and stressing constraints. This study does not delve into the origins of fault complexity, but it is likely that such complexity is influenced by fracture and yielding properties, as well as the maturity of the fault.

182

183

184

185

186

187

188

189

190

191

192

193

194

195

196

197

198

199

200

201

202

203

204

Determining whether slip behavior is primarily governed by rate-and-state type frictional laws or the geometric complexities of fault networks poses a challenging question. The impact of fault geometry continues to be a subject of debate, as various studies have produced conflicting conclusions. Our findings contradict the previous understanding that creep occurs along faults with high roughness, heterogeneous structure and certain compositions<sup>3</sup>. Although creep in subduction zones has been observed to be more prevalent in rough seafloor relief<sup>38</sup>, oceanic transform faults that typically exhibit simpler structures accommodate significant aseismic slip<sup>47,48</sup>. The possibility of effectively modeling the frictional effects of complex fault network geometry within a rate-andstate friction framework can be considered as well. For instance, dynamic simulations have demonstrated that simple geometric complexities, such as overlapping faults, can reproduce slow slip events without the need for complex frictional characteristics on the fault<sup>9</sup>. However, discrepancies in experimental findings regarding frictional behavior at tectonic rates persist, even for well-known minerals like clay<sup>49</sup>, which introduces further uncertainty into the application of rate-and-state friction at geologic conditions, and it remains unclear how a rate-and-state framework would predict our observations. Consensus remains elusive, and it is crucial to gather

more real-world observational evidence to gain a deeper understanding of the complex relationship between fault network geometry, fault friction, and fault slip behavior.

207

208

205

206

### MAIN REFERENCES

- 1. Avouac, J.-P. From geodetic imaging of seismic and aseismic fault slip to dynamic modeling of the seismic cycle. *Annu. Rev. Earth Planet. Sci.* **43**, 233-271 (2015)
- 2. Harris, R. A. Large earthquakes and creeping faults. *Rev. Geophys.* **55**, 169-198 (2017)
- 3. Bürgmann, R. The geophysics, geology and mechanics of slow fault slip. *Earth Planet. Sci.*
- 213 *Lett.* **495**, 112-134 (2018)
- 4. Harbord, C.W., Nielsen, S.B., De Paola, N. & Holdsworth, R.E. Earthquake nucleation on rough faults. *Geology* **45(10)**, 931-934. (2017)
- 5. Eijsink, A.M., Kirkpatrick, J.D., Renard, F. & Ikari, M.J. Fault surface morphology as an indicator for earthquake nucleation potential. *Geology* **50(12)**, 1356-1360 (2022)
- 6. Goebel, T.H., Brodsky, E.E. & Dresen, G. Fault Roughness Promotes Earthquake-Like Aftershock Clustering in the Lab. *Geophys. Res. Lett.* **50(8)**, p.e2022GL101241 (2023)
- 7. Morad, D., Sagy, A., Tal, Y. & Hatzor, Y.H. Fault roughness controls sliding instability.

  Earth Planet. Sci. Lett. **579**, 117365 (2022)
- 8. Bhat, H. S., Olives, M., Dmowska, R., & Rice, J. R. Role of fault branches in earthquake rupture dynamics. *J. Geophys. Res.* **112**, B11309 (2007)
- 9. Romanet, P., Bhat, H. S., Jolivet, R., & Madariaga, R. Fast and slow slip events emerge due to fault geometrical complexity. **45**, *Geophys. Res. Lett.* 4809–4819 (2018)
- 10. Cattania, C. & Segall, P. Precursory slow slip and foreshocks on rough faults. *J. Geophys.*Res. Solid Earth 126, e2020JB020430 (2021)

- 11. Ozawa, S. & Ando, R. Mainshock and aftershock sequence simulation in geometrically
- complex fault zones. *J. Geophys. Res. Solid Earth* **126**, e2020JB020865 (2021)
- 12. Perrin, C., Manighetti, I., Ampuero, J.-P., Cappa, F., & Gaudemer, Y. Location of largest
- earthquake slip and fast rupture controlled by along-strike change in fault structural
- 232 maturity due to fault growth. *J. Geophys. Res. Solid Earth* **121**, 3666–3685 (2016)
- 13. Tsai, V. C. & Hirth, G. Elastic impact consequences for high-frequency earthquake ground
- 234 motion. Geophys. Res. Lett. 47, e2019GL086302 (2020)
- 14. Biasi, G. P. & Wesnousky, S. G. Rupture Passing Probabilities at Fault Bends and Steps,
- with Application to Rupture Length Probabilities for Earthquake Early Warning. Bull.
- 237 Seismol. Soc. Am. 111(4), 2235–2247 (2021)
- 15. Chu, S. X., Tsai, V. C., Trugman, D. T., & Hirth, G. Fault interactions enhance high-
- frequency earthquake radiation. *Geophys. Res. Lett.* **48**, e2021GL095271 (2021)
- 16. Rodriguez Padilla, A. M. Oskin, M. E., Rockwell, T. K., Delusina, I., & Singleton, D. M.
- Joint earthquake ruptures of the San Andreas and San Jacinto faults, California, USA.
- 242 *Geology* **50(4)**, 387–391 (2021)
- 17. Tsai, V. C., Hirth, G., Trugman, D. T., & Chu, S. X. Impact versus frictional earthquake
- models for high-frequency radiation in complex fault zones. J. Geophys. Res. Solid Earth
- 245 **126**, e2021JB022313 (2021)
- 18. Gauriau, J., & Dolan, J. F. Relative structural complexity of plate-boundary fault systems
- controls incremental slip-rate behavior of major strike-slip faults. *Geochem. Geophys.*
- 248 *Geosyst.*, **22**, e2021GC009938 (2021)
- 19. Scholz, C. Earthquakes and friction laws. *Nature* **391**, 37–42 (1998)

- 20. Bizzarri, A. & Bhat, H. S. The Mechanics of Faulting: From Laboratory to Real
- 251 *Earthquakes.* (Research Signpost, 2012)
- 21. Kaneko, Y., Fialko, Y., Sandwell, D. T., Tong, X., & Furuya, M. Interseismic deformation
- and creep along the central section of the North Anatolian Fault (Turkey): InSAR
- observations and implications for rate-and-state friction properties. J. Geophys. Res. Solid
- 255 Earth 118, 316–331 (2013)
- 22. Lockner, D., Morrow, C., Moore, D. & Hickman, S. Low strength of deep San Andreas
- 257 fault gouge from SAFOD core. *Nature* **472**, 82–85 (2011).
- 23. Moore, D. E., and Rymer, M. J. Talc-bearing serpentinite and the creeping section of the
- 259 San Andreas fault. *Nature* **448**, 795–797 (2007)
- 24. Moore, D. E., McLaughlin, R. J. & Lienkaemper, J. J. Serpentinite in a creeping trace of
- the Bartlett Springs Fault, Northern California. Geological Society of America Abstracts
- with Programs, Paper No. 306-3 47(7), 774 (2015)
- 25. Lindsey, E. O., & Fialko, Y. Geodetic constraints on frictional properties and earthquake
- hazard in the Imperial Valley, Southern California. J. Geophys. Res. Solid Earth 121,
- 265 1097–1113 (2016)
- 26. Wei, M., Sandwell, D. & Fialko, Y., A silent Mw 4.7 slip event of October 2006 on the
- Superstition Hills fault, southern California. J. Geophys. Res. 114, B07402 (2009)
- 27. Funning, G. J., Burgmann, R., Ferretti, A., Novali, F., & Fumagalli, A. Creep on the
- Rodgers Creek fault, northern San Francisco Bay area from a 10 year PS-InSAR dataset.
- 270 *Geophys. Res. Lett.* **34**, L19306 (2007)
- 28. Lienkaemper, J. J., McFarland, F. S., Simpson, R. W., & Caskey, S. J. Using surface creep
- rate to infer fraction locked for sections of the San Andreas fault system in northern

- California from alignment array and GPS data. Bull. Seismol. Soc. Am. 104(6), 3094–3114
- 274 (2014)
- 29. Jolivet, R., Candela, T., Lasserre, C., Renard, F., Klinger, Y., et al. The Burst-Like
- Behavior of Aseismic Slip on a Rough Fault: The Creeping Section of the Haiyuan Fault,
- 277 China. Bull. Seismol. Soc. Am. **105(1)**, 480–488 (2014)
- 30. Jolivet, R., Lasserre, C., Doin, M.-P., Peltzer, G., Avouac, J.-P., et al. Spatio-temporal
- evolution of aseismic slip along the Haiyuan fault, China: Implications for fault frictional
- 280 properties. Earth Planet. Sci. Lett. 377–378, 23-33 (2013)
- 31. Li, Y., Bürgmann, R., & Taira, T. Spatiotemporal variations of surface deformation,
- shallow creep rate, and slip partitioning between the San Andreas and southern Calaveras
- Fault. J. Geophys. Res. Solid Earth 128, e2022JB025363 (2023)
- 32. Lindsey, E. O., Fialko, Y., Bock, Y., Sandwell, D. T. and Bilham, R. (2014), Localized and
- distributed creep along the southern San Andreas Fault, *J. Geophys. Res. Solid Earth* **119**,
- 286 7909–7922 (2014)
- 33. Johnson, K. M., Murray, J. R. & Wespestad, C. Creep Rate Models for the 2023 US
- National Seismic Hazard Model: Physically Constrained Inversions for the Distribution of
- 289 Creep on California Faults. *Seismol. Res. Lett.* **93(6)**, 3151–3169. (2022)
- 34. U.S. Geological Survey and California Geological Survey, Quaternary fault and fold
- database for the United States, accessed Sep 26, 2023, at: https://www.usgs.gov/natural-
- 292 hazards/earthquake-hazards/faults.
- 293 35. Mitchell, T.M., & Faulkner, D.R. The nature and origin of off-fault damage surrounding
- strike-slip fault zones with a wide range of displacements: A field study from the Atacama
- fault system, northern Chile, *J. Struct. Geol.* **31(8)**, 802-816 (2009)

- 36. Power, W.L., Tullis, T.E., Brown, S.R., Boitnott, G.N., & Scholz, C.H. Roughness of natural fault surfaces. *Geophys. Res. Lett.* **14**, 29-32 (1987)
- 298 37. Candela, T., Renard, F., Klinger, Y., Mair, K., Schmittbuhl, J., & Brodsky, E.
- E. Roughness of fault surfaces over nine decades of length scales. J. Geophys. Res. Solid
- 300 *Earth* **117**, B08409 (2012)
- 38. Wang, K. & Bilek, S. L. Invited review paper: Fault creep caused by subduction of rough
- seafloor relief. *Tectonophysics*, **610**, 1-24 (2014)
- 39. Reches, Z., & Fineberg, J. Earthquakes as dynamic fracture phenomena. J. Geophys. Res.
- 304 *Solid Earth* **128**, e2022JB026295 (2023)
- 40. Marone, C., & Saffer, D. M. (2007). Fault friction and the upper transition from seismic to
- aseismic faulting. In T. H. Dixon & J. C. Moore (Eds.), The Seismogenic Zone of
- Subduction Thrust Faults (pp. 692). Columbia University Press.
- 41. Holden, C., Kaneko, Y., D'Anastasio, E., Benites, R., Fry, B. & Hamling, I. J. The 2016
- Kaikōura earthquake revealed by kinematic source inversion and seismic wavefield
- simulations: Slow rupture propagation on a geometrically complex crustal fault network.
- 311 *Geophys. Res. Lett.* **44**, 11,320–11,328. (2017)
- 42. Swanson, M. T. Pseudotachylyte-bearing strike-slip faults in mylonitic host rocks, Fort
- Foster brittle zone, Kittery, Maine. In Earthquakes: Radiated Energy and the Physics of
- Faulting Geophysical Monograph Series (Vol. 170, pp. 167–179). Washington, DC:
- 315 American Geophysical Union. (2006)
- 43. Antoine, S. L., Klinger, Y., Delorme, A., & Gold, R. D. Off-fault deformation in regions
- of complex fault geometries: The 2013,  $M_w$ 7.7, Baluchistan rupture (Pakistan). J. Geophys.
- 318 Res. Solid Earth 127, e2022JB024480 (2022)

319	44. Liu YK., Ross, Z. E., Cochran, E. S., & Lapusta, N. A unified perspective of seismicity
320	and fault coupling along the San Andreas Fault. Sci. Adv. 8, eabk1167 (2022)

- 45. Dunham, E. M., Belanger, D., Cong, L., & Kozdon, J. E. Earthquake Ruptures with Strongly Rate-Weakening Friction and Off-Fault Plasticity, Part 2: Nonplanar Faults. *Bull. Seismol. Soc. Am.* **101 (5)**, 2308–2322 (2011)
- 46. Ross, E. O., Reber, J. E., & Titus, S. J. Relating slip behavior to off-fault deformation using physical models. *Geophys. Res. Lett.* **49**, e2021GL096784 ( (2022). )
- 47. Boettcher, M. S., & Jordan, T. H. Earthquake scaling relations for mid-ocean ridge transform faults, *J. Geophys. Res.*, **109**, B12302 (2004)
- 48. McGuire, J., Collins, J., Gouédard, P. *et al.* Variations in earthquake rupture properties along the Gofar transform fault, East Pacific Rise. *Nature Geosci.* **5**, 336–341 (2012)
- 49. Ikari, M. J. & Kopf, A. J. Seismic potential of weak, near-surface faults revealed at plate tectonic slip rates. *Sci. Adv.* **3**, e1701269 (2017)

334

335

336

337

338

339

340

341

321

322

323

333 METHODS

### **Surface Creep Estimates**

We use the compiled surface creep measurements in California<sup>33</sup> to estimate creep rates at regular intervals along major fault segments. We resample surface creep rates from the raw data at 10-kilometer intervals along all of the fault zones (resulting in 208 creep data points) in order to mitigate potential spatial sampling biases, given the concentrated measurements in regions with significant surface creep rates (see Extended Data Fig. 4). Most of the observed fault sections demonstrate right-lateral creep, with a few exceptions along the Bartlett Springs, Maacama, and North Coast San Andreas Fault faults. Based on the absolute values of the estimated creep rates,

we categorize them into two distinct groups: those larger than 3 mm/year, referred to as "creeping", and those smaller, referred to as "locked". To check whether our results are sensitive to the precise value of this creep categorization cutoff, we test other values of the cutoff from 1 to 5 mm/yr and find that our results are insensitive to such differences in cutoff choice (see Extended Data Fig. 5a). We define normalized creep rates by dividing observed surface creep rates by the cumulative seismic moment for all earthquakes with magnitudes larger than 1 within a 15-km radius area during 1980-2022.

# **Fault Misalignment and Fault Density**

For each point with a creep rate estimate, we calculate the misalignment ratio of the fault strands within a 15-km radius circle using the surface fault traces from the USGS Quaternary Faults Database<sup>34</sup>. We determine fault misalignments by calculating the ratio of the minimum and maximum length of the summed fault trace projections for every possible rotation angle<sup>15</sup>. The misalignment ratio represents the extent of misaligned faults in the area, with a value of zero indicating perfectly parallel fault strands and a value of one indicating random fault orientations. We also examine the potential correlation with fault density, defined as the sum of fault lengths within an area divided by the length of the perimeter. We assume that measurements of fault complexity using surface fault traces are adequate for shallow depths, where surface creep is commonly observed and attributed to fault properties, but note that there may be uncertainties introduced related to this assumption. Geodetic studies have suggested that surface creep rates can extend to depths ranging from 5 to 15 km, depending on the specific creeping fault system<sup>50,51</sup>.

While our measurements of fault network complexity encompass both fault density and fault misalignment, we concentrate our study on fault misalignment and not on fault density primarily because fault density displayed minimal to no correlation with surface creep rates (see Extended Data Fig. 1c). This lack of correlation with fault density may be attributable to the poorer scaling properties of fault density compared to fault misalignment. While fault misalignment remains independent of fault map resolution for a fractal fault geometry, fault density increases with higher-resolution fault maps<sup>15</sup>. Therefore, our measurements of fault misalignment made at the kilometer scale are more likely to remain valid at smaller, relevant scales (see Extended Data Fig. 5b) whereas areas with high fault density may be inaccurately measured as having low fault density due to the limitations of fault map resolution. This inconsistency may account for the little or no correlation observed between fault density and fault creep.

### The North Anatolian Fault and the Chaman Fault

To demonstrate that the correlation between surface creep rates and fault misalignment is not only limited to faults in California, but may be a common behavior for other creeping faults globally, we examine two additional, well-documented faults: the North Anatolian Fault and the Chaman Fault. The Ismetpasa and Izmit segments of the North Anatolian Fault are known to be slipping aseismically, with surface creep rates of up to 1 cm/yr, while the Bolu-Gerede segment is identified as being locked<sup>52</sup>. Using surface creep rates derived from InSAR measurements<sup>53,54</sup>, we estimate the surface creep rates at sampled locations along different segments of the North Anatolian Fault. Sampling was conducted at intervals of 0.4° in longitude, focusing only on faults known to be locked or where surface creep rate measurements are available. Surface creep rates were prescribed as 0 mm/yr at segments known to be locked. The fault misalignments at these

sampled locations were calculated within 18-km radius circles, using active faults with confidence levels of 'A' and 'B' from the Active Faults of Eurasia Database<sup>55</sup>.

For the Chaman fault, several segments including the Nushki segment, are known to exhibit creeping behavior, with surface slip rates ranging from 5 to 10 mm/yr<sup>56-58</sup>. We use the Map of Quaternary faults in Afghanistan<sup>59</sup> to calculate fault misalignment within 18-km radius circles. Only the fault section between 29° and 32° N was considered, due to large uncertainties regarding the creeping or locking behavior of the northern segments. The choice of 18-km radius circles was somewhat arbitrary to capture significant fault complexities around the sample points. In the analysis of both faults, surface creep rates derived from InSAR data were smoothed by computing a 40-km average for each sample point to reduce noise. For the Chaman fault, reliable measurements with uncertainties smaller than the mean uncertainty of 1.7 mm/yr were used for average creep rate estimation<sup>56</sup>. We note that variations in the sampling distance or in the radius size did not significantly affect the observed trend.

### DATA AND CODE AVAILABILITY

The surface creep data used in this study is available from Johnson et al. (2022) (<a href="https://www.usgs.gov/data/creep-rate-models-california-faults-2023-us-national-seismic-hazard-model">https://www.usgs.gov/data/creep-rate-models-california-faults-2023-us-national-seismic-hazard-model</a>). The surface fault traces are from the USGS Quaternary Fault Database (<a href="https://www.usgs.gov/programs/earthquake-hazards/faults">https://www.usgs.gov/programs/earthquake-hazards/faults</a>). The earthquake catalog data can be downloaded from NCEDC and SCEDC. Codes used in this research are available on Zenodo at <a href="https://doi.org/10.5281/zenodo.10982013">https://doi.org/10.5281/zenodo.10982013</a>.

- 50. Chaussard, E., Bürgmann, R., Fattahi, H., Johnson, C. W., Nadeau, R., Taira, T., &
- Johanson, I. Interseismic coupling and refined earthquake potential on the Hayward-
- 411 Calaveras fault zone, *J. Geophys. Res. Solid Earth* **120**, 8570–8590 (2015)
- 412 51. Murray, J. R., S. E. Minson, & J. L. Svarc. Slip rates and spatially variable creep on
- faults of the northern San Andreas system inferred through Bayesian inversion of Global
- 414 Positioning System data. J. Geophys. Res. Solid Earth, 119, 6023–6047 (2014)
- 52. Kaduri, M., Gratier, J.-P., Renard, F., Çakir, Z., & Lasserre C. The implications of fault
- zone transformation on aseismic creep: Example of the North Anatolian Fault, Turkey. J.
- 417 *Geophys. Res. Solid Earth*, **122**, 4208–4236 (2017)
- 418 53. Aslan, G., Lasserre, C., Cakir, Z., Ergintav, S., Özarpaci, S., Dogan, U., et al. Shallow
- creep along the 1999 Izmit earthquake rupture (Turkey) from GPS and high temporal
- resolution interferometric synthetic aperture radar data (2011–2017). J. Geophys. Res.
- 421 *Solid Earth.* **124**, 2218–2236 (2019)
- 54. Jolivet, R., Jara, J., Dalaison, M., Rouet-Leduc, B., Özdemir, A., Dogan, U., et al. Daily to
- 423 centennial behavior of aseismic slip along the central section of the North Anatolian Fault.
- 424 J. Geophys. Res. Solid Earth, 128, e2022JB026018. (2023)
- 425 55. Zelenin, E., Bachmanov, D., Garipova, S., Trifonov, V., & Kozhurin, A.: The Active Faults
- of Eurasia Database (AFEAD): the ontology and design behind the continental-scale
- dataset. Earth Syst. Sci. Data, 14, 4489–4503 (2022)
- 56. Dalaison, M., Jolivet, R., van Rijsingen, E. M., & Michel, S. The interplay between
- seismic and aseismic slip along the Chaman fault illuminated by InSAR. J. Geophys. Res.
- 430 *Solid Earth* **126**, e2021JB021935 (2021)

449	ACKNOWLEDGEMENTS		
448			
447	Behavior". Zenodo. doi:10.5281/zenodo.10982013 (2024)		
446	63. Lee, J. Data and Code for "Fault Network Geometry Influences Earthquake Frictional		
445	doi:10.7909/C3WD3xH1 (2013)		
444	62. SCEDC : Southern California Earthquake Center. Caltech. Dataset.		
443	Laboratory. Dataset. doi:10.7932/NCEDC (2014)		
442	61. NCEDC: Northern California Earthquake Data Center. UC Berkeley Seismological		
441	https://doi.org/10.6028/NIST.IR.6453 (Accessed October 10, 2023)		
440	National Institute of Standards and Technology, Gaithersburg, MD, [online],		
439	60. Fenimore, C., Libert, J. & Brill, M. Algebraic constraints implying monotonicity for cubics :		
438	Survey Open-File Report 2007-1103, (2007)		
437	database of probable and possible Quaternary faults in Afghanistan: U.S. Geological		
436	59. Ruleman, C.A., Crone, A.J., Machette, M.N., Haller, K.M., & Rukstales, K.S. Map and		
435	8406 (2016)		
434	along the Chaman Fault system, Pakistan and Afghanistan. Geophys. Res. Lett. 43, 8399-		
433	58. Fattahi, H., & Amelung, F. InSAR observations of strain accumulation and fault creep		
432	from InSAR, J. Geophys. Res. Solid Earth. 122, 372–386 (2017)		
431	57. Barnhart, W. D. Fault creep rates of the Chaman fault (Afghanistan and Pakistan) inferred		

The work presented in this paper was supported by National Science Foundation grants

450

451

EAR-2146640 and EAR-2231705.

### **AUTHOR INFORMATION**

453	
454	
455	Dep
456	029
457	Jaes

**Authors and Affiliations** 

Department of Earth, Environmental, and Planetary Sciences, Brown University, Providence, RI

02912, USA

Jaeseok Lee, Victor C Tsai, and Greg Hirth

Nevada Seismological Laboratory, University of Nevada, Reno, Reno, NV 89557, USA

Avigyan Chatterjee and Daniel T. Trugman

460

461

462

463

464

465

466

467

468

458

459

### **Contributions**

VCT conceived and designed the study, JL led the investigation, including data analysis, visualization, and interpretation. DTT and AC contributed to the statistical analysis and interpretation of fault complexity and creep rate data. GH helped with the interpretation of results in the framework of rock mechanics and frictional theory. JL took the lead in drafting the manuscript. All authors provided input on the analysis, reviewed the results, contributed to editing the manuscript and approved the final version of the manuscript. VCT, DTT and GH secured funding to support the project.

469

470

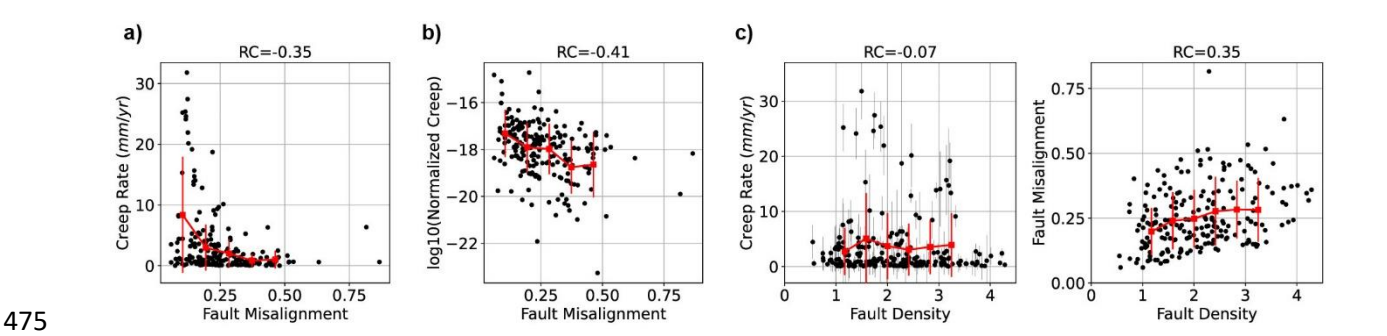
471

472

#### AUTHOR STATEMENT

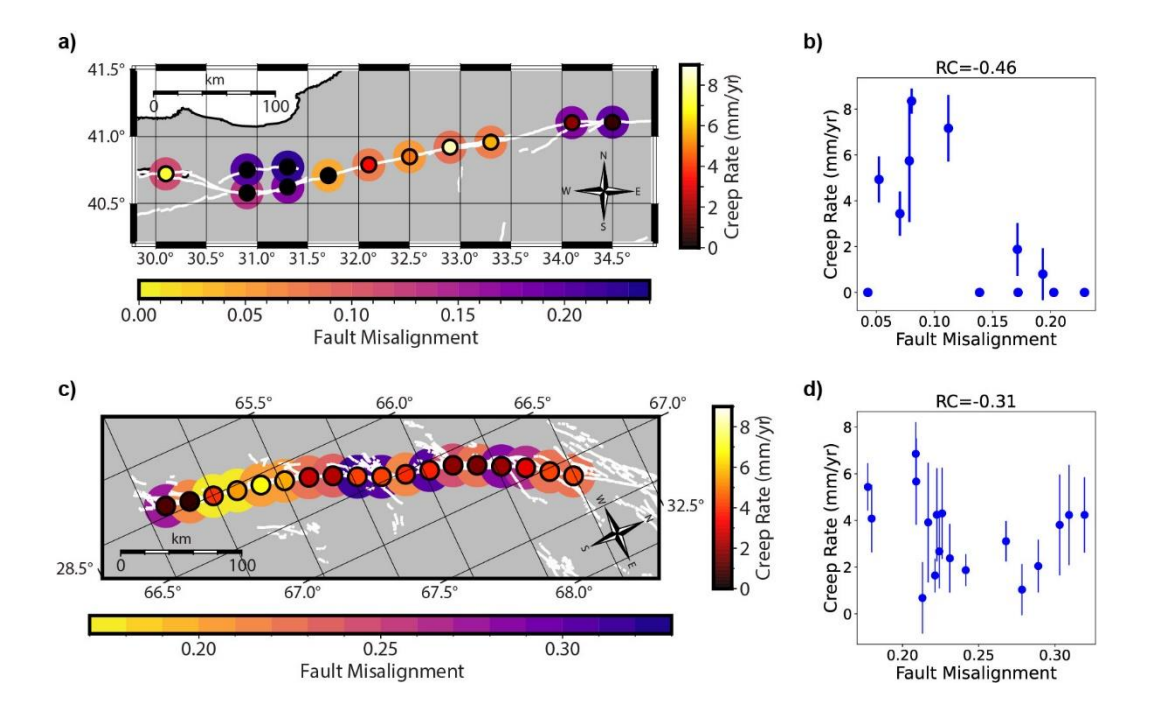
The authors declare no financial or non-financial competing interests. Correspondence and requests for materials should be addressed to Victor C. Tsai at <victor tsai@brown.edu>.

# **EXTENDED DATA FIGURES**

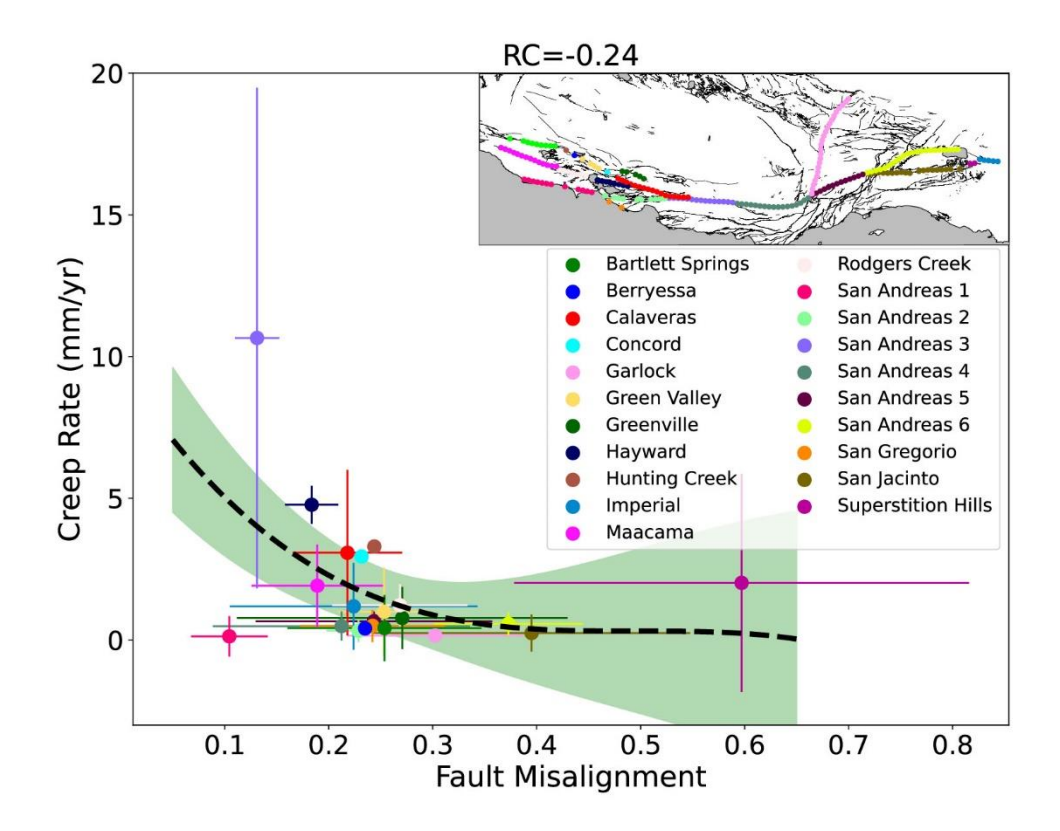


Extended Data Figure 1. Scatter plots for fault misalignment and fault density. a,

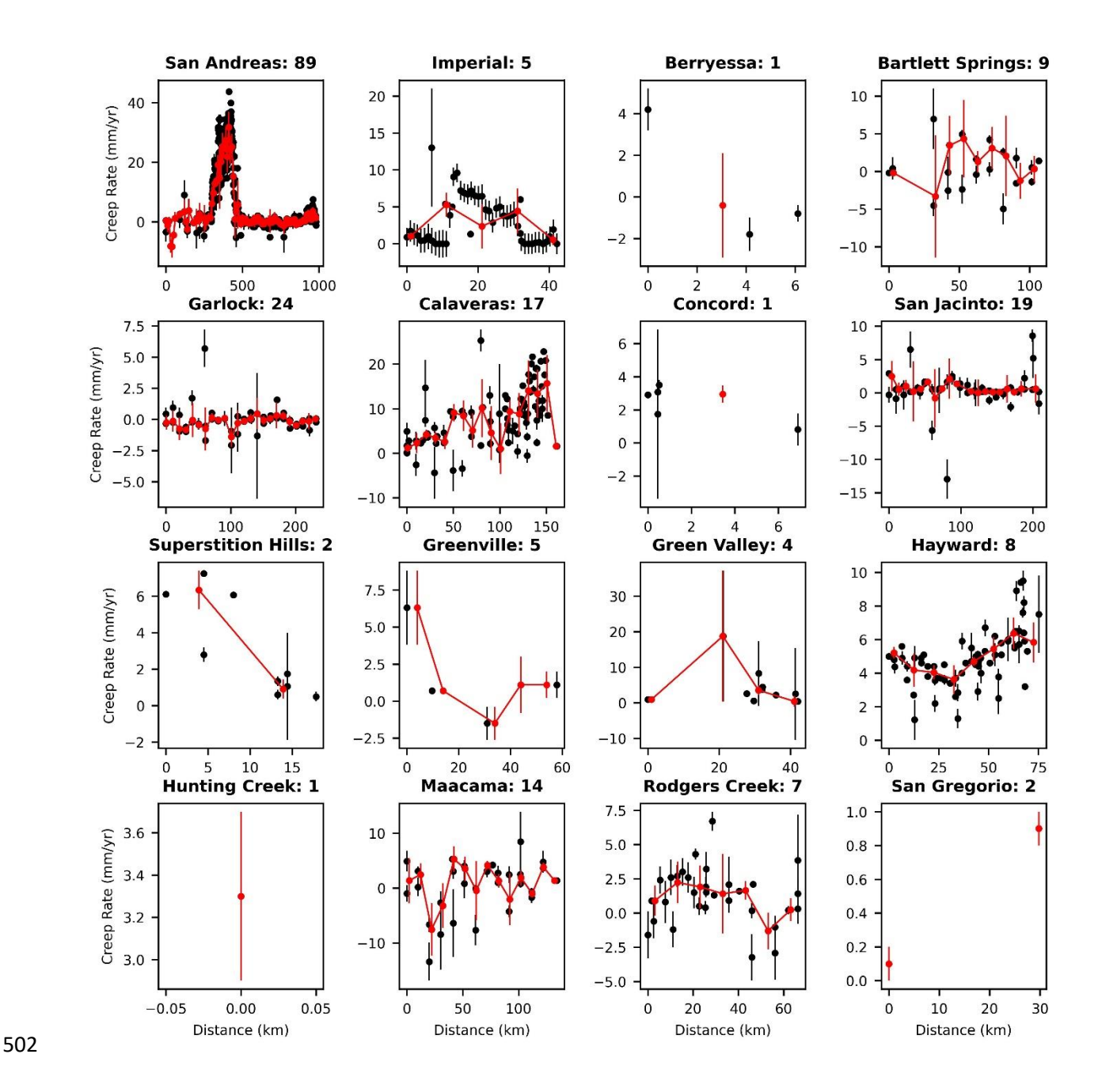
Scatter plot of surface creep rate versus fault misalignment. **b,** Scatter plot of surface creep rate normalized by accumulated seismic moment versus fault misalignment. The negative correlation between fault misalignment and normalized creep remains consistent. **c,** Scatter plot of surface creep rate and fault misalignment versus fault density. Fault density correlates with fault misalignment, but does not show any correlation with creep rates. **a, b, c,** Spearman's rank correlation (RC) coefficients between the variables are in the subplot titles, and the red error bar plots indicate the means and standard deviations for the binned intervals.



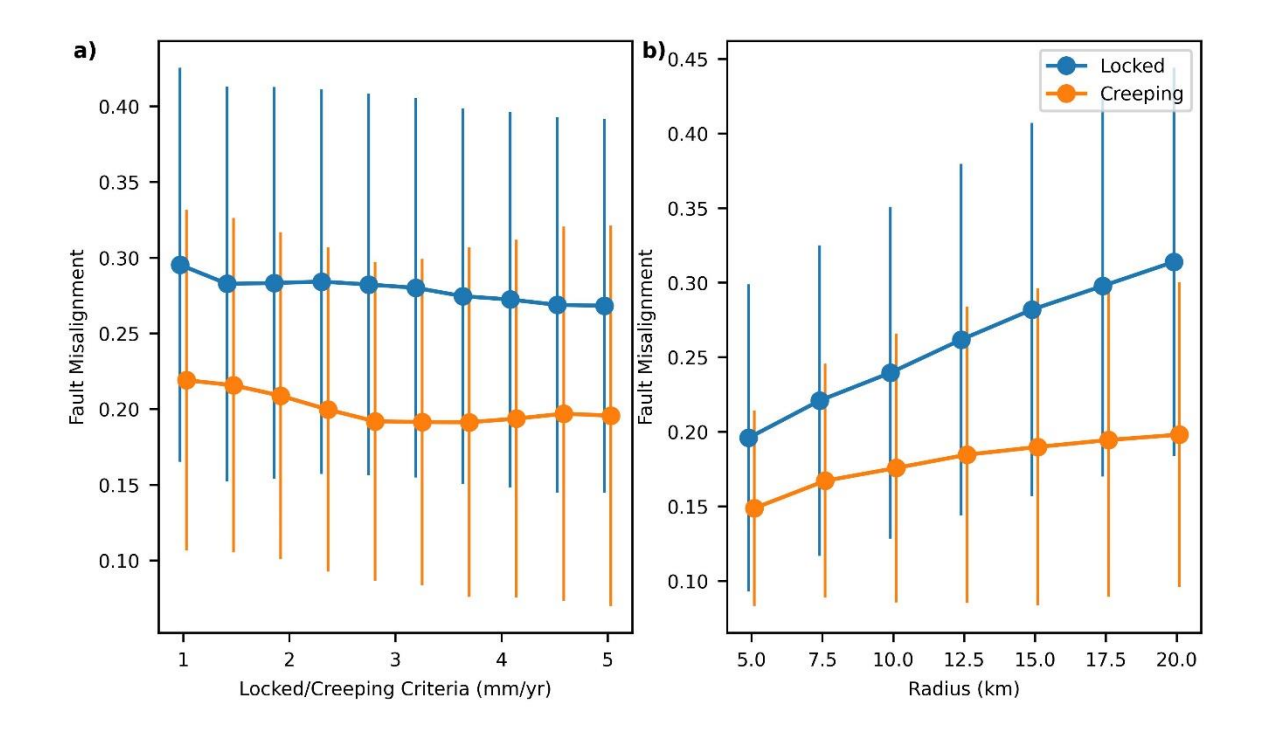
Extended Data Figure 2. Fault misalignment and creep outside California. a, Fault misalignment and fault creep rate along the North Anatolian Fault. Inner circles indicate surface creep rates<sup>52-54</sup> and outer circles indicate measured fault misalignments. Surface fault traces are colored in white<sup>55</sup>. b, Scatter plot of fault misalignment and surface creep rates along the North Anatolian Fault. Spearman's rank correlation (RC) coefficient between the two is indicated in the subplot title. c, Fault misalignment and fault creep rate along the Chaman Fault. Inner circles indicate surface creep rates<sup>56</sup> and outer circles indicate measured fault misalignments. Surface fault traces are colored in white<sup>59</sup>. d, Scatter plot of fault misalignment and surface creep rates along the Chaman Fault. Spearman's rank correlation (RC) coefficient between the two is indicated in the subplot title.



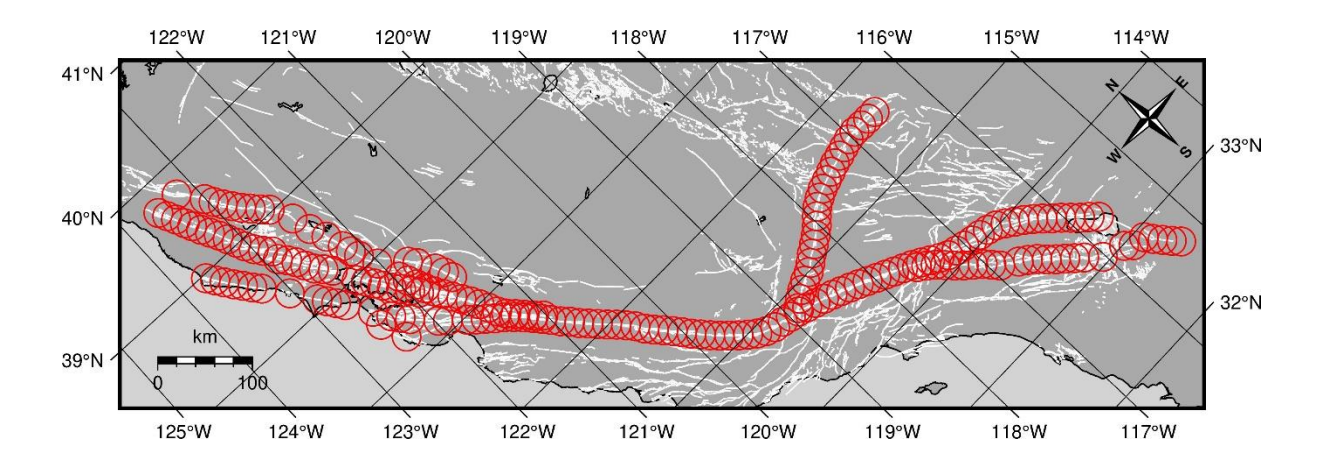
Extended Data Figure 3. Average surface creep rates and fault misalignment for different fault segments in California. Spearman's rank correlation (RC) coefficient between the two is indicated in the subplot title, and the black dashed line indicates a monotonic cubic polynomial of best fit.<sup>60</sup>. The green shaded area is a 95% confidence interval around the best fit. The inset map in the upper right corner depicts the fault segments using the same colors as in the main plot.



**Extended Data Figure 4. Creep rate sampling.** Comparison of surface creep rates sampled at 10 km intervals along faults in California (red) with the compiled measurements from ref. 33 (black). The number of estimates for each fault are indicated in the subplot titles. Estimates and errors at the sampled locations are calculated as the weighted average of measurements within 10 km.



**Extended Data Figure 5**. **Tests of robustness. a,** Variation in the mean and standard deviation of fault misalignment for locked and creeping faults for different creep cutoff thresholds. **b,** Changes in the mean and standard deviation of fault misalignment for locked and creeping faults (threshold: 3 mm/year), considering various radius circles for measuring fault network misalignment. The distinct distribution of fault misalignment between locked and creeping faults remains consistent, regardless of the chosen cutoff threshold or radius circle used to measure fault complexity. As the radius increases, the fault misalignment in creeping faults with simple geometries remains relatively constant. In contrast, for locked faults with complex geometries, fault misalignment increases due to the violation of the fractality assumption at smaller scales, attributed to limited resolution.



**Extended Data Figure 6. Fault metric regions.** Fault metrics are computed within the red circles.